II.J.3 Value-Added Hydrogen Generation with CO_2 Conversion

Richard Billo (Primary Contact) and
Krishnan Rajeshwar
The University of Texas at Arlington
College of Engineering, Box 19019
Arlington, TX 76019
Phone: (817) 272-2708
E-mail: richard.billo@uta.edu

DOE Managers
HQ: Richard Farmer
Phone: (202) 586-1623
E-mail: Richard.Farmer@ee.doe.gov
GO: Paul Bakke
Phone: (720) 356-1436
E-mail: Paul.Bakke@go.doe.gov

Contract Number: DE-FG36-08GO88170

Project Start Date: August 15, 2008
Project End Date: August 30, 2011

Fiscal Year (FY) 2011 Objectives

TASK 1: Develop Homogeneous Ruthenium Photocatalysts for H_2 Production and CO_2 Reduction

- Synthesis of ruthenium-polypridyl complexes (RPCs) as photocatalysts.
- Screen RPCs for electroctalytic activity.
- Evaluate the photophysical properties of the RPCs.
- Demonstrate photocatalytic CO_2 reduction with RPCs.
- Optimize photocatalytic reaction.

TASK 2: Develop Hetergeneous Oxide Photocatalysts for H_2 Production and CO_2 Reduction

- Develop new oxide semiconductors for photocatalysis and photoelectrochemical catalysis.
- Demonstrate combustion synthesis of $BiVO_4$, Bi_2WO_6, and $AgBiW_2O_6$ nanoparticles.
- Demonstrate photoreduction of CO_2 using $BiVO_4$ nanoparticles.
- Develop method for photodeposition of Pt on $AgBiW_2O_6$.
- Optimizing Bi_2WO_6 and $AgBiW_2O_6$ for CO_2 photoreduction.

This project addresses the following technical barriers from the Production section (3.1) of the Fuel Cell Technologies Program Multi-Year Research, Development and Demonstration Plan:

Task 1: Technical Barriers Addressed

(D) Feedstock Issues
(E) Greenhouse Gas Emissions

Task 2: Technical Barriers Addressed

(Y) Materials Efficiency
(Z) Materials Durability
(AA) PEC Device and System Auxiliary Material
(AB) Bulk Material Synthesis

Technical Targets

Progress towards meeting Technical Targets for CO_2 Use as a Feedstock and Greenhouse Gas Remission

Task 1

- Synthesis of three ruthenium polypyridyl complexes.
- Proof-of-concept demonstration of CO_2 reduction to methanol using electrochemical and photochemical methods.

Task 2

- Combustion Synthesis of $BiVO_4$, Bi_2WO_6, and $AgBiW_2O_6$ nanoparticles.
- Photodeposition of Pt on $AgBiW_2O_6$ nanoparticles to enhance electron-hole separation under irradiation.
- Photocatalytic reduction of CO_2 using Pt-modified $AgBiW_2O_6$

FY 2011 Accomplishments

Task 1

- Prepared two photocatalysts containing a ruthenium chromophore linked to pyridyl moiety.
- Demonstrated that these photocatalysts are competent for CO_2 electroreduction to methanol with an optimum performance at pH of 2.0.
- Demonstrated that the two new photocatalysts are capable of CO_2 photoreduction to methanol but that they require a mixed MeCN-water solvent to function.

Task 2

- Prepared $BiVO_4$, Bi_2WO_6, and $AgBiW_2O_6$ nanoparticles by Combustion Synthesis.
- Demonstrated that the combustion synthesized nanoparticles possess higher photocatalytic performance

and larger surface area than those obtained by solid state reaction.

- Demonstrated the photocatalytic generation of H_2 and reduction of CO_2 using Pt-modified $AgBiW_2O_6$ nanoparticles.

Introduction

Given the current environmental concerns over CO_2 as a greenhouse gas and the need for fuels derived from renewable energy sources, the capture and reduction of CO_2 into fuels could help alleviate the environmental issue and turn this cheap and common feedstock into valuable fuels. The combustion of these fuels would regenerate CO_2 which could, in theory, be 'recycled' into fuel, leading to a closed carbon-cycle. Of course, there is a required energy input for this carbon-based fuel cycle, and ideally this would be based on solar-energy. Task 1 of this project describes the development of molecular photocatalysts, based on the discovery of Bocarsly and co-workers that pyridine is an excellent electrocatalyst for the reduction of CO_2 to methanol [1-3]. In this work, we covalently link a ruthenium chromophore to a pyridine co-catalyst to develop a homogeneous CO_2 reduction photocatalyst. The project involves the design, synthesis, characterization and testing of these photocatalysts for CO_2 reduction to methanol. Task 2 describes the preparation of $BiVO_4$, Bi_2WO_6 and $AgBiW_2O_6$ semiconductor nanoparticles by a "mild" (low-temperature) combustion synthesis. This method is both energy- and time-efficient because the exothermicity of the combustion reaction provides the energy for the synthesis and the reaction times are just few minutes. The resulting combustion synthesized nanoparticles are tested as photocatalyts for H_2 generation and CO_2 reduction. Sample characterization involves several techniques such as high resolution transmission electron microscopy, thermogravimetric analysis, Brunauer-Emmett-Teller (BET) surface area, diffuse reflectance spectroscopy, X-ray diffraction (XRD) and X-ray photoelectron spectroscopy (XPS).

Approach

Task 1

We designed and prepared complexes in which the well-established photochemistry of ruthenium-polypyridyl coordination complexes is used to generate a reduced pyridine functional group. These complexes are characterized electrochemically and photochemically to determine optimum reaction conditions. Excitation of each Ru(II) complex with visible light in the region of 400-500 nm forms an excited ^{1}MLCT (metal-to-ligand charge-transfer) state in which the pyridine-containing ligand is reduced by one electron. This excited state quickly relaxes to a second, long-lived, triplet excited state, ^{3}MLCT. Reductive quenching of the Ru^{3+} center traps the electron on the pyridyl ligand and thus has 'photogenerated' an analogue of the pyridine radical. Reaction of this radical anion with CO_2 at the proper pH leads to a sequence of photoreductions that ultimately produce methanol. We used electrochemistry to screen the photocatalysts for electrocatalytic CO_2 reduction activity under various pH conditions. Gas chromatography coupled with mass spectrometry was used to look for the reduced CO_2 products, specifically for methanol. The complexes ability function as photocatalysts was examined in a custom designed photoreactor with 470 nm ultrabright diode lamp. Reaction conditions included the presence of a sacrificial donor, triethanolamine (TEOA) to reductively quench the photoexcited complexes.

Task 2

We used solution combustion synthesis (SCS) to prepare $BiVO_4$, Bi_2WO_6 and $AgBiW_2O_6$ semiconductor nanoparticles. The selection of these three materials was based on their respective band gap energy overlapping the solar spectrum and thus making them able to perform heterogeneous photoreactions using solar light. Using SCS is very convenient as compared with the traditional solid-state reaction method for nanoparticles preparation. The combustion synthesis uses a fuel (i.e. urea) that in contact with the metal precursors promotes the combustion reaction in few minutes instead of the high energy consumption associated with the solid state reaction that normally takes several hours of heating at high temperatures. Furthermore, SCS generates much smaller nanoparticles because of the gases generated during the combustion reaction. The synthesized powders were characterized in their physical shape and size (high-resolution transmission electron microscopy [HRTEM], BET), composition, crystalline structure (XRD, energy dispersive X-ray spectroscopy, XPS), and light absorption (diffuse reflectance ultraviolet-visible spectroscopy [UV-Vis]). The ability of these nanoparticles as heterogeneous photocatalysts was examined in a 200 mL photoreactor containing 0.5 g of semiconductor nanoparticles in aqueous media irradiated from a light source (xenon or tungsten halogen lamp) placed in an inner Pyrex glass compartment.

Results

Task 1

We prepared the three photocatalysts shown in Figure 1 in 90% yield and have characterized them by nuclear magnetic resonance and elemental analysis. They are isolated as the hexafluorophosphate salt for solubility in acetonitrile or as chloride salt for solubility in water.

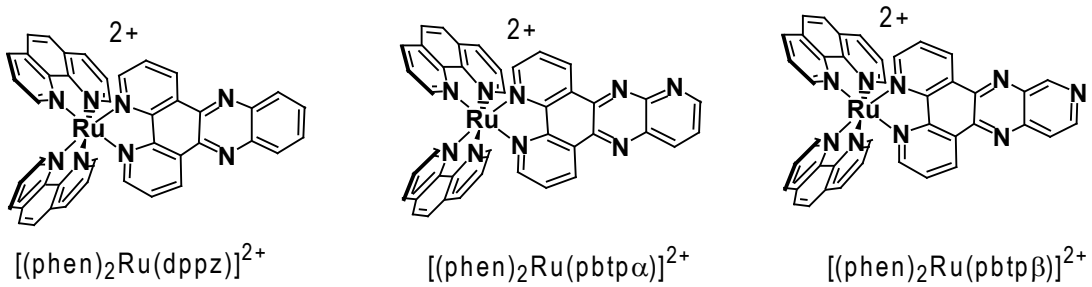

FIGURE 1. Structures of RPCs Described in Task 1

Electrochemistry

The voltammetric behavior of $[(bpy)_2Ru(ptpb\alpha)]^{2+}$ and $[(bpy)_2Ru(ptpb\beta)]^{2+}$ complexes in the presence of CO_2 is compared in Figure 2. It is worth noticing that both profiles are similar in shape although $[(bpy)_2Ru(ptpb\beta)]^{2+}$ is peaking at less negative potentials than its analog $[(bpy)_2Ru(ptpb\alpha)]^{2+}$ indicating a more facile interaction with CO_2 for the first complex. In both cases, the formation of a reactive nitrogen site in the pbpb (either α or β) ligand for CO_2 adduct formation in the form of a carbamate is expected. Figure 2 also shows that a neat increase of current is occurring at potentials more negative than -1.1 V for both complexes indicating that a next electron uptake is also a possible center for photocatalytic CO_2 reduction. This point is important in the view of the photochemical reduction of CO_2 as the ^{1}MLCT excitation of the Ru π→ ptpb dπ band in any of the complexes and reductive quenching of the ^{3}MLCT excited state by triethylamine could trap the electron on the ptpb ligand to form $[(bpy)_2Ru^{II}(ptp\beta^{-})]^{+}$ either in the bpy structure of the ptpb or at the farther N of the structure. The two different locations in the ptpb ligand might work properly in the photochemical reaction. In relation to the returning positive-going scan in Figure 2, it is clear that anodic currents are much smaller than those shown in the absence of CO_2 and pointing out to a chemical reaction of CO_2 with the reduced product of any of the complexes.

For the mechanistic aspects of the electrochemical reaction, the pH dependence of the electrocatalysis was examined. As shown in Figure 3, the reduction potential shifts positive as the pH is lowered as expected for a proton-coupled process. A 60 mV shift positive for every pH unit is in agreement with a one proton-one electron process. A separate measurement of the pK_a of the pyridine acid in $[(bpy)_2Ru(pbtp\beta)]^{2+}$ revealed a pK_a near 2.0 which corresponds nicely with the peak potential shift observed for the cathodic peak. Using this data and the findings by Bocarsly that pyridine electrocatalysis of CO_2 reduction works best at the pKa of the pyridine acid, we ran all subsequent photoreductions at pH 2 for complexes $[(bpy)_2Ru(ptpb\alpha)]^{2+}$ and $[(bpy)_2Ru(ptpb\beta)]^{2+}$ [3].

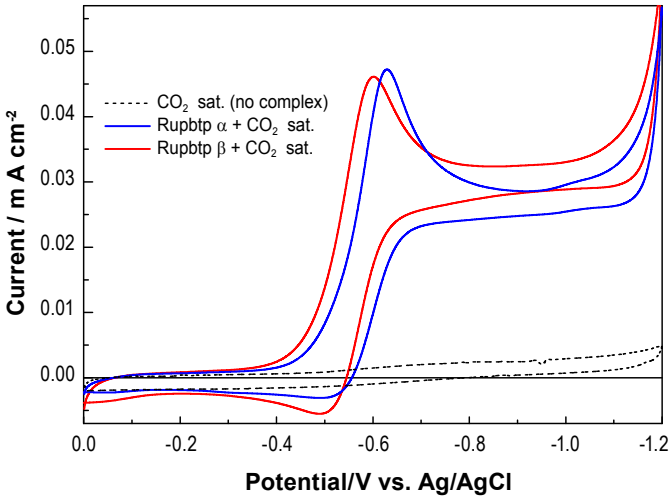

FIGURE 2. Comparison of the voltammetric behavior of $[(bpy)_2Ru(ptpb\alpha)]^{2+}$ and $[(bpy)_2Ru(ptpb\beta)]^{2+}$ in CO_2 saturated solution. Scan rate = 5 mV/s. The voltammogram of CO_2 in the absence of any complex is shown in black dot line.

Photochemistry and Photocatalysis

We examined the ability of $[(bpy)_2Ru(ptpb\alpha)]^{2+}$ and $[(bpy)_2Ru(ptpb\beta)]^{2+}$ to serve as photocatalysts for CO_2 reduction under a variety of conditions. As expected from the literature, pure water solutions were not practical as the excited state lifetime is too short for photoreactions [4]. Solvent mixtures of dimethylformamide (DMF)/water and acetonitrile (MeCN)/water resulted in suitable excited-state lifetimes for the photocatalysts. In a typical experiment, a water jacketed reaction vessel of 50 mL total volume was filled with ~25 mL MeCN that is 1.0 M H_2O, 0.20 M TEOA, and 100 μM Ru complex. The solutions are degassed and then placed in a homemade photochemical reactor in which blue light irradiation of wavelength 470 nm is provided by ultra bright diode array setup. Samples of both the headspace and solution are collected at various time periods and subjected to gas chromatographic (GC) analysis for product detection.

GC data was collected using a Haysep DB packed column with a length of 3 m and used N_2 as a carrier gas (starting at 110°C, a temperature ramp of 1°C/minute

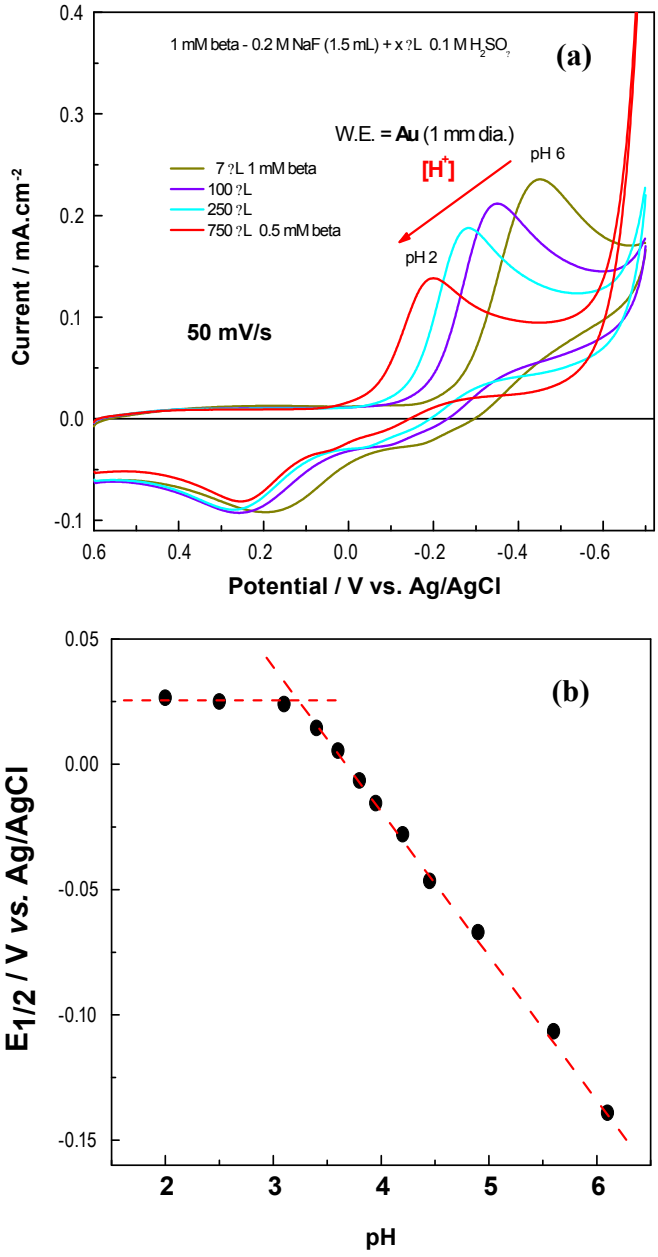

FIGURE 3. a) Selected voltammograms of $[(bpy)_2Ru(pbtp\beta)]^{2+}$ (1 mM) in aqueous media showing the effect of pH on the peak potential associated to the first electroreduction process. b) Linear shift of the half-wave potential ($E_{1/2}$) as a function of the solution pH.

temperature was done immediately after sample injection to a final temperature of 150°C). Retention times were as follows: carbon monoxide, 0.80 min.; methane, 0.88 min.; methanol, 5.8 min.; formaldehyde and formic acid, 8 min.

Methanol was detected under electrolytic and photolytic conditions. Methanol production increased with electrolysis time as expected. In the electrolysis experiment, conditions were 5 mM $[(bpy)_2Ru(pbtp\beta)]^{2+}$, 0.1 M KCl electrolyte, pH 2.0, constant CO_2 bubbling. Constant current at -0.45 mA was applied to a Pt working electrode using a Pt counter

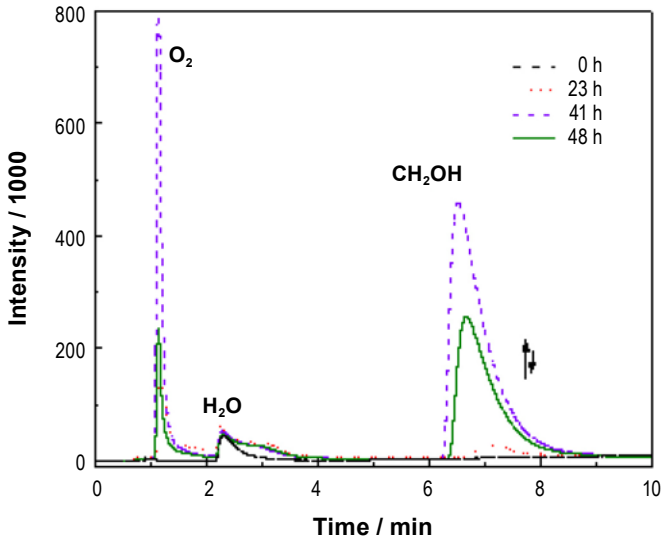

FIGURE 4. Selected GC runs of samples (liquid phase) taken during the $Ru(phen)_2pbtp\beta^{2+}$ + CO_2 electrolysis.

electrode in a separate compartment, and Ag/AgCl reference electrode in the working electrode compartment. These results are only semi-quantitative due to peak overlap in the gas chromatogram and need further refinement for yields and turnover numbers. Similarly, methanol was detected in a photochemical experiment. In a typical experiment, a water jacketed reaction vessel of 50 mL total volume was filled with ~25 mL MeCN or DMF that is 1.0 M H_2O (pH 2), 0.20 M ascorbic acid, and 100 mM Ru complex. The solutions are degassed, saturated with CO_2, and then placed in the photochemical reactor for irradiation at 470 nm. Samples of both the headspace and solution were collected at various time periods and subjected to GC analysis for product detection. Methanol was detected by GC of the solution phase (Figure 4) and its identity confirmed by mass spectrometry. As with the electrolysis result, the results are not quantitative as overlap of the MeOH peak with another species prevents accurate quantification. Work is in progress to find conditions for clear resolution of the MeOH peak by GC.

Task 2

$BiVO_4$, Bi_2WO_6 and $AgBiW_2O_6$ nanoparticles were prepared by SCS [5]. The band edges of these three semiconductor materials are shown in Figure 5 comparatively to other materials and also the redox potentials for CO_2 electroreduction and water splitting are shown there. The three selected materials have band gaps in the 2.4-2.7 eV range thus overlapping the solar spectrum and in contrast with TiO_2 which has served as a model workhorse for a stable and inert inorganic semiconductor although its 3.2 eV band gap is too high to be used as solar absorber.

All samples were fully characterized (by HRTEM, XPS, XRD, BET, UV-Vis and Raman spectroscopy) to ascertain

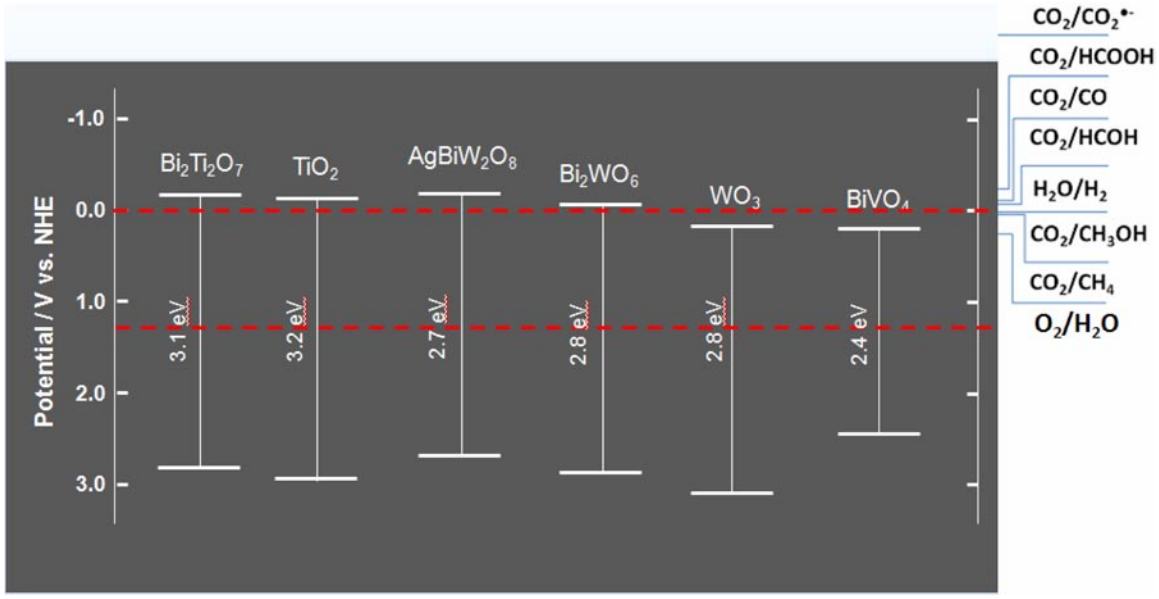

FIGURE 5. Comparison between the band edges of selected semiconductors (at pH 1) and the redox potentials for CO_2 reduction and water splitting.

particle size, composition, crystalline structure and absence of impurities [6]. Figure 6 shows the UV-visible diffuse reflectance data on a SCS-synthesized $AgBiW_2O_6$ sample processed in the form of Tauc plot of the square root of the Kubelka–Munk function vs. the photon energy. The band gap value estimated from this plot is 2.73 eV and in very good agreement with the value (2.75 eV) reported for this ternary oxide in a previous study on solid-state reaction

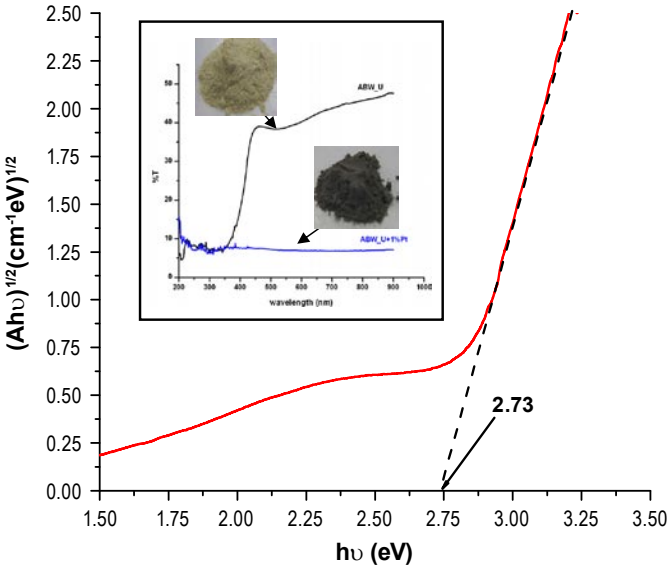

FIGURE 6. Tauc plot for combustion synthesized $AgBiW_2O_8$. The inset shows the percent transmittance data of the sample before (black line) and after photodeposition of 1wt% Pt (blue line), along with the corresponding sample photographs.

(SSR) [7]. Much higher surface areas (as determined by BET isotherm, see Table 1) are found for the SCS samples than for those prepared by SSR, thus pointing out to a better quality product obtained in a time- and energy-efficient manner by SCS.

TABLE 1.

Photocatalyst	Micropore Area (cm^2)	External Surface Area (cm^2)	BET Surface Area ($m^2\ g^{-1}$)
SCS $AgBiW_2O_8$	5.488	28.938	34.44 (our work)
SSR $AgBiW_2O_8$	0.136	0.406	0.54 (our work)
SSR $AgBiW_2O_8$	-	-	0.29 (ref. 7)

A newly designed sealed photoreactor was then used to perform heterogeneous photocatalysis with the semiconductor particles suspended in CO_2 saturated water. The lamp (400 W medium-pressure Hg arc encased in Pyrex glass, photon flux: 235 mW/cm^2) was turned on and the gaseous products evolved were analyzed by gas chromatography (GC SRI 310) as a function of the illumination time using a Shin Carbon column and a thermal conductivity detector.

Best samples for photoreduction of CO_2 are the SCS-derived $AgBiW_2O_8$ powders which are able to perform the photocatalytic generation of syngas followed the principle outlined in Figure 7a. The rationale for using formate ions as the in situ precursor for CO_2 was two-fold. The direct electroreduction of CO_2 in aqueous media is beset both by the low partial pressure of CO_2 in the atmosphere (3.9×10^{-4} atm) and by its low solubility in water (1.5 g/L at

298 K) [8]. On the other hand, formate species have high solubility in water (945 g/L at 298 K) [9]; they have high proclivity for being adsorbed on oxide surfaces and are easily photoconverted to CO_2 (Figure 7a). The in situ generated CO_2 can be subsequently reduced by the photogenerated electrons in the oxide particle. For the simultaneous photogeneration of H_2, the photogenerated electrons must be stored on the oxide surface in noble metal catalyst (e.g., Pt) islands [10]. Thus, the $AgBiW_2O_8$ particles were loaded with 1 mass% Pt using a photocatalytic procedure described elsewhere [11]. After surface modification with Pt, the color of the oxide particles changed significantly from light yellow to a grayish hue as illustrated in Figure 6 (insert). The diffuse reflectance spectra also changed consequently as also shown in Figure 6 (insert). Thus, we envision that the portion of the photogenerated electrons channeled toward the Pt catalyst islands would reduce protons to hydrogen while those that diffuse to the (naked) oxide surface would be utilized for the reduction of CO_2 to CO (Figure 7a).

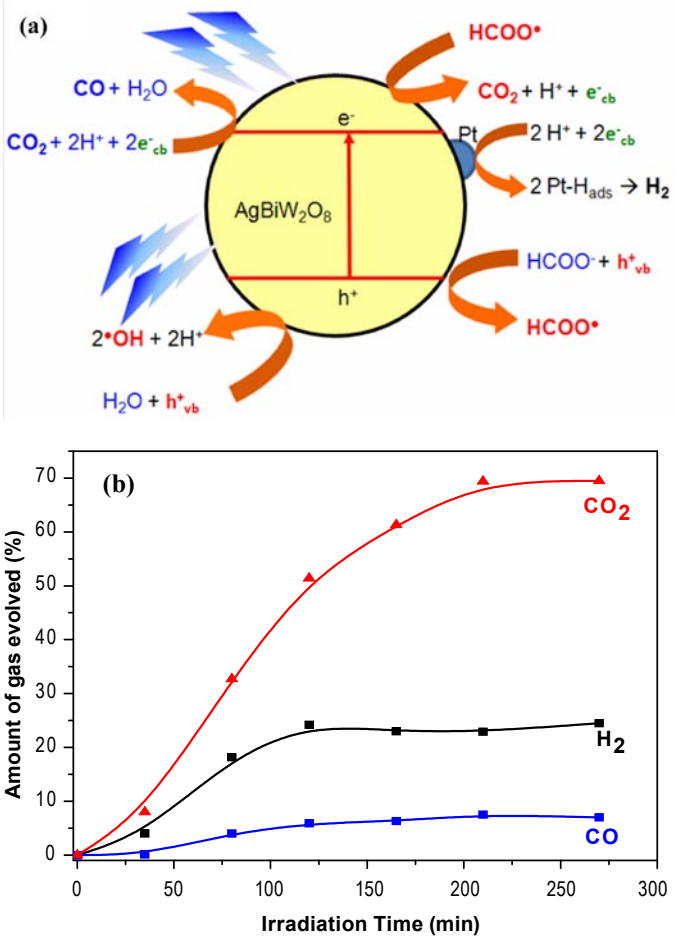

FIGURE 7. a) Diagram of heterogeneous photocatalytic formation of syngas on an illuminated AgBiW2O8-Pt nanoparticule. b) Amount of gas evolved (H2 and CO) as a function of irradiation time using in situ CO_2 generation from 0.1 M HCOOH.

The Pt-modified $AgBiW_2O_8$ particles were loaded into the photoreactor containing a de-aerated solution of 0.1 M HCOOH at a dose of 2 g/L. Figure 7b illustrates the temporal profiles of the three products of the overall photocatalytic reaction, namely, H_2, CO and CO_2. It is worth noting that the first products to be seen are the generation of CO_2 and H_2 from the oxidation of HCOOH using the photogenerated holes from the semiconductor valence band and the reduction of H^+ through photogenerated electrons in the conduction band of $AgBiW_2O_8$ respectively. The (subsequent) formation of CO tracks the in situ photogeneration of CO_2 at or near the particle surfaces. The run was terminated at 225 min at which time the gases accumulated were as follows: $H_2 = 1.0 \times 10^{-2}$ mol/gL, $CO = 3.0 \times 10^{-3}$ mol/gL and $CO_2 = 2.8 \times 10^{-2}$ mol/gL. These data are reported as the number of moles of product divided by the photocatalyst mass and liquid volume in the photoreactor. Quantum yields for the formation of syngas (H_2+CO) and CO_2 in the formic acid solution amount to $H_2 = 3.0$ %, $CO = 0.8$ % and $CO_2 = 4.5$ %.

Conclusions and Future Directions

Our findings in Task 1 show that properly designed RPCs can act as a homogeneous photocatalyst or electrocatalyst for CO_2 reduction to methanol. This proof of concept now needs to be refined and optimized to determine the efficiency of the process. Ultimately, we would need to couple the reductive process with a more practical oxidative process, for example water oxidation, to construct a practical system for solar fuel generation.

Our findings in Task 2 show that among the three heterogeneous photocatalysts, the Pt-modified $AgBiW_2O_8$ is capable of performing CO_2 photoreduction. The data described is a useful proof-of-concept for the following: (a) $AgBiW_2O_8$ can be simply and quickly prepared by SCS; (b) A mild photocatalytic procedure for syngas generation can be developed based on the use of formate ions as an in situ precursor for CO_2, and (c) The SCS-derived $AgBiW_2O_8$ powder, after Pt surface modification, can generate syngas via this procedure. Ultimately, better performances can be expected by optimizing the amount of Pt on the semiconductor nanoparticles and by using solvent mixtures of DMF/water and MeCN/water to enhance CO_2 solubility in the liquid phase.

References

1. Barton, C.E.; Lakkaraju, P.S.; Rampulla, D.M.; Morris, A.J.; Abelev, E.; Bocarsly, A.B. *J. Am. Chem. Soc.* **2010**, *132*, 11539-11551. 10.1021/ja1023496.

2. Barton, E.E.; Rampulla, D.M.; Bocarsly, A.B. *J. Am. Chem. Soc.* **2008**, *130*, 6342-6344. 10.1021/ja0776327.

3. Seshadri, G.; Lin, C.; Bocarsly, A.B. *J. Electroanal. Chem.* **1994**, *372*, 145-150.

4. Nair, R.B.; Cullum, B.M.; Murphy, C.J. Optical Properties of [Ru(phen)(2)dppz](2+) as a Function of Nonaqueous Environment. *Inorg Chem* **1997**, *36*, 962-965.

5. Rajeshwar, K.; de Tacconi, N.R. *Chem. Soc. Rev.* **2009**, *38*, 1984 - 1998.

6. Timmaji, H.K.; Chanmanee, W.; de Tacconi, N.R.; Rajeshwar, K. *J. Adv. Oxid. Technol.* **2011**, *14*, 1-13.

7. Tang, J.; Ye, J. *J. Mater. Chem.* **2005**, *15*, 4246 - 4251.

8. Palmer, D. A.; Van Eldik, R. *Chem. Rev*. **1983**, *83*, *651* - 731.

9. *CRC Handbook of Chemistry and Physics*, 82nd Edition, CRC Press: Boca Raton, FL, **2001-2002.**

10. Rajeshwar, K. *J. Appl. Electrochem.* **2007**, *37*, 765 - 787.

11. de Tacconi, N. R.; Chenthamarakshan, C. R.; Rajeshwar, K., Lin, W-Y.; Carlson, T.; Nikiel, L.; Wampler, W.A.; Sambandam, S.; Ramani, V. *J. Electrochem. Soc.* **2008**, *155*, B1102 – B1109.